eXPRESS Polymer Letters Vol.14, No.7 (2020) 619–637
Available online at www.expresspolymlett.com
https://doi.org/10.3144/expresspolymlett.2020.51

Ionic transport studies of solid bio-polymer electrolytes based on carboxymethyl cellulose doped with ammonium acetate and its potential application as an electrical double layer capacitor

N. M. J. Rasali[1], *M. A. Saadiah*[1,2], *N. K. Zainuddin*[1], *Y. Nagao*[3], *A. S. Samsudin*[1*]

[1]Ionic Material Team, Faculty of Industrial Sciences and Technology, Universiti Malaysia Pahang, 26300 Pahang, Malaysia
[2]Department of Chemistry, Centre for Foundation Studies, International Islamic University Malaysia, 26300 Gambang, Pahang, Malaysia
[3]School of Materials Science, Japan Advanced Institute of Science and Technology, 1-1 Asahidai, Nomi, 923-1292 Ishikawa, Japan

Received 5 September 2019; accepted in revised form 15 November 2019

Abstract. CMC-$NH_4CH_3CO_2$ complexes were characterized via theoretical and experimental approaches using molecular dynamics (MD) calculation, Fourier transform infrared spectrometry (FTIR), X-ray diffraction (XRD), and electrical impedance spectroscopy (EIS) analysis. These analyses successfully disclosed the structural and ion conduction properties of the bio-polymer electrolytes (BPE) system. The FTIR analysis further revealed that an interaction exists between the carboxylate anion group (COO^-) from CMC and the H^+ substructure of $NH_4CH_3CO_2$. The ionic conductivity value at ambient temperature was found to achieve an optimum value of 5.07×10^{-6} S/cm for a system containing 10 wt% $NH_4CH_3CO_2$. The ionic conductivity improvement was demonstrated via the increment on the amorphous phase of the BPEs system as shown in the XRD analysis upon the inclusion of $NH_4CH_3CO_2$. Based on the IR-deconvolution approach, the mobility (μ) and diffusion coefficient (D) were found to influence the ionic conductivity and aligned with the theoretical molecular dynamic (MD) calculation. To evaluate the potential application of the CMC-$NH_4CH_3CO_2$, an electrical double-layer capacitor (EDLC) was fabricated from the BPE and tested using cyclic voltammetry (CV), and charge-discharge (GCD) for 300 cycles and the BPE exhibited a specific of capacitance ~2.4 F/g.

Keywords: *biopolymers, theoretical approach, ionic conductivity, transport properties, electrochemical properties*

1. Introduction

Since Armand [1] discovered that polymers could be utilized as solid electrolyte systems, solid polymer electrolytes (SPEs) have played an important role in its application to electrochemical devices [2–6]. This is notably due to their unique properties, such as the capability to accommodate a various range of ionic dopants, desirable electrode-electrolyte connection, favorable ionic conductivity, and the ease of forming it into thin films that could deliver high energy density. However, the electrolyte materials are important components and must be chemically stable under all operating conditions since the main role of the electrolytes is to transport ions. The vast majority of current research works in electrolytes system have targeted the encompassing of synthetic polymers such as polyethylene oxide (PEO) [5, 7], polycarbonate [8], polymethylmethacryalate [9], and polysiloxane

*Corresponding author, e-mail: ahmadsalihin@ump.edu.my

[10]. Although synthetic polymers possess excellent mechanical and conductivity performance, their preparation involves toxic and volatile organic compounds (VOCs), which may lead to serious environmental issues. Therefore, the search for novel and alternative environmentally friendly host polymers with better performance as a solid electrolyte system is still an emerging issue in the field of solid state research.

Among polymers that are derived from natural sources, various families of natural polymers have been studied such as chitosan, starch, carrageenan, pectin, agarose, and cellulose. According to Zainuddin and Samsudin [6], kappa carrageenan which is a polysaccharide offers relatively higher conductivity within a magnitude of ~10^{-7} S/cm. Besides, [11] has found that agarose derived from red seaweed can serve as a potent BPE candidate, with a much higher conductivity of ~10^{-4} S/cm. Furthermore, Ramesh *et al*. [9] has carried out research on tamarind seed polysaccharide for use as a BPE and found that the conductivity value was 5.48×10^{-8} S/cm. Another study on proton-conducting BPE based on pectin has reported a conductivity value of 2.68×10^{-9} S/cm [12]. Chitosan was also evaluated as a BPE by Alves *et al*. [13], who found that its conductivity was 3.64×10^{-7} S/cm at ambient temperature. The authors have indicated that by an introduction of appropriate ionic dopant, the conductive nature of the insulating biopolymer can be improved for potential use in electrochemical applications.

Many studies have chosen cellulose and its derivative, nanocellulose, as host materials in electrolyte systems due to its semi-crystalline nature (modification of cellulose) [14, 15]. Cellulose and nanocellulose are claimed to be emerging renewable materials to replace the use of non-biodegradable petroleum-derived materials [16]. Cellulose is abundant in nature as it accounts for one–third of the Earth's vegetative matter [17], with an estimated worldwide production of 10^{10} and 10^{11} tons per year [18]. The application of cellulose has received considerable attention in fuel cells [19], biomedical engineering [20], wastewater treatment of textile industry [21] and food industry [22]. Figure 1 shows the chemical structure of cellulose which consists of repeating units of glucose, and it is a linear natural polymer consisting of 1,4-anhydro-D-glucopyranose units [23]. The beneficial properties of cellulose that include biocompatibility, abundance, renewability, biodegradability,

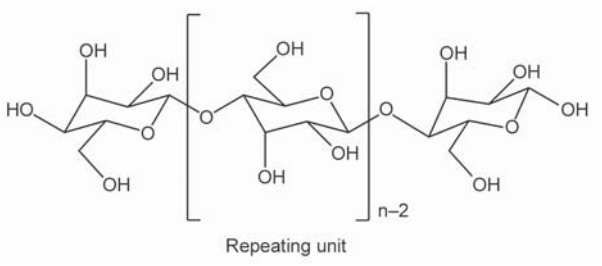

Figure 1. Chemical structure of cellulose [26].

non–abrasive nature in processing, and high specific mechanical strength amongst others make cellulose to be one of the most promising candidates for use in energy storage devices [24, 25].

The present work is an attempt to enhance the electrochemical properties of the carboxymethyl cellulose (CMC) as it is an excellent candidate for the development of conducting materials as a BPE. Previous studies have also been conducted by several researchers that revealed the conducting behavior of the CMC [27–30]. Generally, CMC is a cellulose derivative that has been extensively used in a diverse array of applications, such as food additives, textiles fibers, adhesives, paints, pharmaceuticals, cosmetics, and medical supplies [31]. CMC is a highly water-soluble material made of an anionic polysaccharide that consists of β-1.4-linked anhydro-D-glucose units bearing hydroxyl (–OH) and carboxylate ($–COO^-$) groups. These properties cause CMC to be an excellent candidate as a biopolymer electrolyte for applications in energy storage devices. The electrical double-layer capacitor (EDLC) is one of the alternative energy storage devices which has greater ability to store large amounts of energy than a regulator capacitor. The function of the EDLC is based on the movement of ions that is present in the electrolyte when exposed to fixed voltage. Besides, the mechanism involved in the EDLC is completely non-faradaic which does not involve any electron exchange [32]. EDLC was also reported to demonstrate higher power density, higher reversibility and long life cycle [33].

Much research has been done to convert non-conducting biomaterials into conducting materials with tailored individual properties well-suited to energy storage devices. Simple modifications of the CMC are expected to offer outstanding properties that exhibit good mechanical and thermal integrity, favorable conductivity, superior thermostability (decomposition temperature is up to 250 °C), and also a wide electrochemical stability window [24, 34–36].

In the present study, the ion conduction properties of the CMC-$NH_4CH_3CO_2$ BPE system, was investigated via theoretical and experimental approaches. It is, therefore, anticipated that BPEs based on cellulose derivatives, specifically CMC, could replace commercial synthetic polymers for a more sustainable future. The results obtained from this analysis were used to correlate the structural properties and ionic conductivity of the CMC-$NH_4CH_3CO_2$. The highest conducting BPE was used as the electrolyte in the fabrication of an EDLC for the evaluation of the potential window of the electrolyte, specific capacitance and cycle characteristics.

2. Experimental

2.1. Materials and sample preparation

CMC sodium salt (M_w ~ 90 000; Density ~ 1.59: Acros Organic Co.) and $NH_4CH_3CO_2$ (M_w ~ 77.08; Density ~ 1.17: Merck Co.) were obtained. The CMC-$NH_4CH_3CO_2$ sample was prepared via the solution casting technique. Firstly, 2 g of CMC was dissolved into distilled water, and different amounts in weight percentage (wt%) of $NH_4CH_3CO_2$ were added into the CMC solution. The mixtures were stirred continuously until they were homogenous. The mixtures were then cast into Petri dishes and dried in an oven at 60 °C until films formed. Then, the films were left in desiccators for additional drying. The schematic preparation of sample, sample designation and physical appearance of the films are shown in Figure 2.

Composition of CMC-$NH_4CH_3CO_2$ in BPEs system

Sample	CMC [g]	$NH_4CH_3CO_2$ [wt%]
1	2.0000	0
2		5
3		10
4		15
5		20
6		25

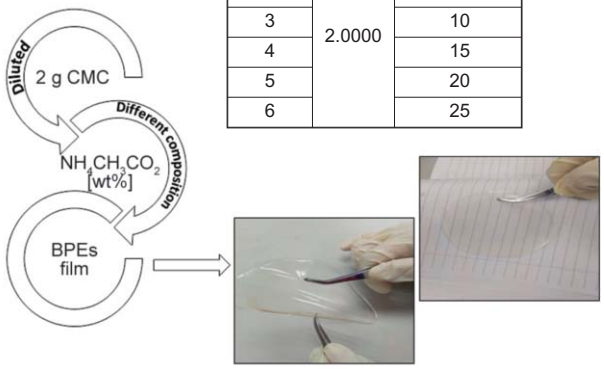

Figure 2. Schematic diagram of the preparation of CMC-$NH_4CH_3CO_2$ films.

2.2. Characterization of the CMC-$NH_4CH_3CO_2$ BPE system

2.2.1. Fourier transform infrared (FTIR) spectroscopy

The CMC-$NH_4CH_3CO_2$ BPE complexes were studied using FTIR spectroscopy using a Thermo Nicolet 380 equipped with ATR and Germanium crystal. The resulting BPEs produced were examined directly using the Germanium crystal and does not require any sample preparation. The samples were characterized with a resolution of 2 cm^{-1} and wavenumber ranging from 700 to 4000 cm^{-1}. The infrared radiation could induce molecular vibrations, which include bending and stretching at the covalent bonds particularly [37].

2.2.2. IR spectra deconvolution

The IR deconvolution was carried out using the Origin Lab 8.0 software via the Gaussian-Lorentz function. Peaks at the selected regions were chosen based on the complexation revealed by the FTIR analysis. After the baseline was determined, the IR spectra were deconvoluted, and the peaks were fitted using the software to separate regions of free ions and contact ions. From the deconvolution of IR spectra, the area under the curve corresponds to the area of free ions and contact ions, which is useful for further calculation. The free ions percentages were calculated using Equation (1) [38–41]:

$$\text{Free ions} = \frac{A_f}{A_f + A_c} \cdot 100\% \tag{1}$$

where A_f is the area under the curve for free ions, and A_c is area under the curve that represents the contact ions. The number (η), mobility (μ) and diffusion coefficient (D) of ions were calculated using Equations (2)–(4) [41]:

$$\eta = \frac{M \cdot N_a}{V_T} \cdot \text{Free ions } [\%] \tag{2}$$

$$\mu = \frac{\sigma}{\eta q} \tag{3}$$

$$D = \frac{k_B T \mu}{e} \tag{4}$$

where N_a is Avogadro's number, M is the number moles of $NH_4CH_3CO_2$, V_T is the total volume of CMC-$NH_4CH_3CO_2$ BPE sample, k_B is the Boltzmann constant (1.38×10^{-23} $m^2\cdot kg\cdot s^{-2}\cdot K^{-1}$), T is the

absolute temperature (303 K) in Kelvin [K] unit, and q is the electron charge (1.602×10^{-19} C).

2.2.3. X-ray diffraction (XRD)

X-ray diffraction (XRD) spectra of the CMC-$NH_4CH_3CO_2$ BPEs system were attained using a Rigaku MiniFlex II Diffractometer. The prepared sample was scanned at 2θ angles between 5 and 80° that was equipped with a CuKα source.

The data analysis was carried out using the Origin Lab 8.0 software. The area under the peak was identified, and the degree of crystallinity was computed by using Equation (5) [42]:

$$X_c = \frac{A_c}{A_c + A_a} \cdot 100\% \tag{5}$$

where A_c is the area of crystalline part and A_a is the area of the amorphous region.

2.2.4. Electrical impedance spectroscopy (EIS)

The ionic conductivities of the CMC-$NH_4CH_3CO_2$ BPEs system were characterized via a HIOKI 3532-50 LCR Hi-Tester in a frequency range of 50 Hz to 1 MHz at the temperature of 303 K. The electrolytes were sandwiched between two stainless steel electrodes. Based on the impedance data, the real impedance, Z_r, and imaginary impedance, Z_i, were calculated by using the Equations (6) and (7):

$$Z_r = \frac{\cos\left(\frac{\pi p}{2}\right)}{k^{-1}\omega p} \tag{6}$$

and

$$Z_i = \frac{\sin\left(\frac{\pi p}{2}\right)}{k^{-1}\omega p} \tag{7}$$

The k^{-1} variable corresponds to the capacitance value of the *CPE* element, ω is the angular frequency, and p is referred to as the deviation of the vertical axis in the Z_r *versus* Z_i plot. By referring to the plot of imaginary impedance (Z_i) versus real impedance (Z_r), the bulk modulus (R_b) can be determined and further applied in the Equation (8) below for conductivity determination:

$$\sigma = \frac{y}{R_b} \cdot \frac{1}{A} \tag{8}$$

where R_b is the bulk resistance, A [cm^2] is the contact area, and y is the thickness of BPE samples.

2.2.5. Molecular dynamics (MD) analysis

The VIOVIA Materials Studio 2017 software package (Dassault Systems) was used for the molecular dynamics (MD) analysis. Before MD calculation, as components for calculation, the 7-mer of CMC and $NH_4CH_3CO_2$ were built and structurally optimized by DFT calculation using the DMol3 software's Perdew–Burke–Ernzerhof (PBE) function. The convergence threshold for the maximum force and maximum displacement for standard geometry optimization were set to 0.02 Ha Å^{-1} and 0.05 Å, respectively. For MD calculation, four amorphous cells with a different amount of $NH_4CH_3CO_2$ were built by the Amorphous Cell module using a COMPASS II force field. To minimize energy in each system, an NVT ensemble was performed for 100 ps by the Forcite module using the COMPASS II force field. After annealing structure, the NVE ensemble was performed for 1000 ps using COMPASS II at 300 K. The mean square displacements of all ammonium ions were analyzed as averages by Forcite Analysis.

2.2.6. Transference number measurement (TNM)

TNM was performed using Wagner's DC polarization method to prove the ion conduction in the BPEs system [40, 43]. The DC was monitored as a function of time on the application of a fixed dc voltage (1.5 V) across the sample mounted between two stainless steel electrodes.

2.2.7. Voltammetry measurement

Linear sweep voltammetry (LSV) measurements were performed using a C–H instrument potentiostat to study the electrochemical stability window of the electrolytes at room temperature. LSV measurements were carried out at a scan rate of 2 mV·s^{-1} at room temperature with the voltage range of 0–3 V.

2.2.8. EDLC fabrication and characterization

In order to determine the possibility of applying the CMC-$NH_4CH_3CO_2$ BPE in electrochemical devices, the fabrication of an electrical double-layer capacitor (EDLC) was carried out. Activated carbon, (Black Powder, BP20), conductive super powder carbon black (super P), and polvinylidene fluoride (PVDF) in the ratio of 80:10:10 were first thoroughly mixed. Then, the mixture was ground using mortar and

pestle, and 4.0 ml of *N*-methyl-2-pyrrolidone (NMP) was added to obtain a slurry. The slurry was then spread onto aluminum foil which was used as the current-collector. The electrode was heated at 100 °C in a vacuum oven overnight before being used. The electrode was then cut into circles with size of 1.77 cm^2. The BPE with the highest ionic conductivity was sandwiched between two graphite sheet electrodes and placed inside a coin cell. The fabricated EDLC was then tested for cyclic voltammetry and charge-discharge measurements. The CVs tested were measured at different scan rates from 0 to 1 V. The specific capacitance, C_s of the EDLC was calculated from the CV using the Equation (9) [44]:

$$C_s = \int_{V_1}^{V_2} \frac{I(V)}{2(V_2 - V_1)mv} dV \quad (9)$$

where $I(V)$ is current, m is mass of active material, $(V_2 - V_1)$ is the potential voltage and v is the applied scan rate.

The NEWARE galvanostatic charge-discharge (GCD) software was used to evaluate the electrochemical performance of the highest conducting BPE in an assembled EDLC cell. Charge – discharge measurement was done using a BTS battery cycler with a voltage range of 0 to 1 V at a different constant current. The C_s of discharge characteristic, equivalent series resistance (ESR), coulombic efficiency and η [%] of the EDLC can be determined using the equations found in the literature [45–48].

3. Results and discussion

3.1. Bio-polymer complexes analysis

In FTIR analyses, molecular vibrations vary according to the materials used. Different functional groups are expected to exhibit different vibration modes with different intensities [49]. In cellulose, stretching and bending are commonly found in the IR spectra. Stretching vibration causes the inter-atom distance along the bond to change whereas bending results in the change of bond angle [50]. Figure 3 presents the composition of all samples of BPEs system in the 700 to 1700 cm^{-1} region. The absorption peaks for CMC have been reported in previous literature [51–54]. Four absorption peaks appear at 1597, 1428, 1331, 1063 cm^{-1}, which corresponded to COO^- asymmetric, O–H bending, C–H stretching, and C–O–C bending respectively. These four peaks are characteristic fingerprint bands for pure CMC which was in agreement with Saadiah *et al*. [55], Samsudin and Isa [56], further Sohaimy and Isa [57]. However, further complexity may be observed in the IR spectra based on the addition of various $NH_4CH_3CO_2$ compositions.

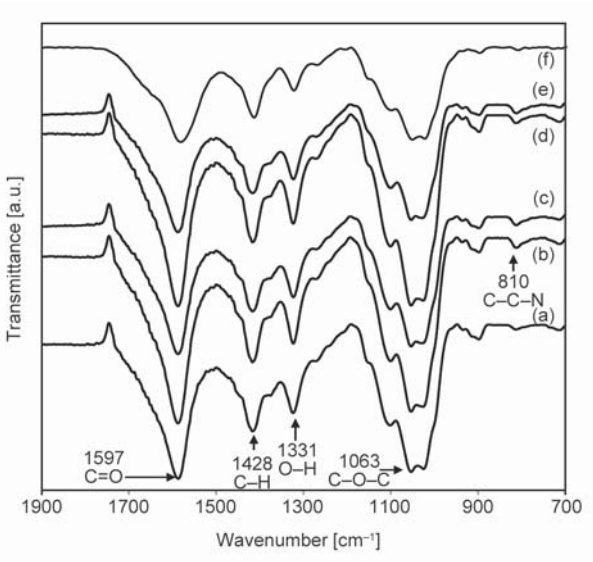

Figure 3. FTIR spectra of samples (a) 1; (b) 2; (c) 3; (d) 4; (e) 5 and (f) 6 of CMC-$NH_4CH_3CO_2$ BPEs system in the 700 to 1900 cm^{-1} region.

It was noticed that starting from sample 2 , an obvious hump was observed at the 810 cm^{-1} region that corresponded to the C–C–N stretching, which confirmed the incorporation of $NNH_4CH_3CO_2$ [58]. It is also suggested that complexation of $NH_4CH_3CO_2$ with CMC had taken place with respect to the bending of the beta-1,4-glucosidic (C–O–C) in CMC due to the peak shifting from 1063 cm^{-1} to a lower wavenumber of 1059 cm^{-1} as reported in the previous literature [40–43]. Complexation of $NH_4CH_3CO_2$ and CMC was driven by van der Waals forces due to the oxygen in the –COC– creating a polarized region that attracts the H^+ from $NH_4CH_3CO_2$ via dipoles-dipoles interaction [59].

In this work, the migration of H^+ to COO^- is possible. As reported by Ng and Mohamad [81], the most labile bond of H^+ is from the four hydrogen bonds (NH_3–H^+) that can easily dissociate and hop from the coordinating site to other sites on the CMC host which allows conduction of the electrical field. These reactions are possible since in the tetrahedral structure of NH_4^+, two of the four hydrogen atoms are bonded identically while the third is bound firmly. In accordance with previous studies, the present study also demonstrated a similar complexation which was observed at the 1600 cm^{-1} region that corresponded to the favorable complexation of CMC and $NH_4CH_3CO_2$ that involved the COO- group and H^+.

It was observed that the carboxylate group (–COO^-) at 1597 cm^{-1} had shifted to a lower wavenumber of 1582 cm^{-1} with a concomitant decrease in peak intensity after the introduction of $NH_4CH_3CO_2$ into the BPEs system. Changes were expected and are believed to occur at 1597 cm^{-1} due to the interaction between H^+ from NH_4^+ of $NH_4CH_3CO_2$ via a hopping mechanism. Apparently, the increment of $NH_4CH_3CO_2$ in CMC had resulted in a higher concentration of H^+ that was dissociated from NH_4^+. Thus, an electrostatic attraction was expected between the H^+ and –COO^- in the CMC and this was demonstrated by the shifting in wavenumber and changes in the peak's intensity.

It is encouraging to note that the interaction in the C–O–C mode was smaller in comparison to the COO^- mode as projected by a small shift in the former and a strong absorption mode in the latter as reported by Samsudin *et al*. [43] and Biswal and Singh [60]. The result of the present study corroborates with these earlier reports where the C–O–C region exerts weaker van der Waals interaction on the H^+. Meanwhile, the $NH_4CH_3CO_2$ and CMC are believed to have a stronger interaction between the H^+ and the coordinating site (COO^-) group in the CMC as proposed in Figure 4. Thus, we consider the CMC to be a good host polymer in a polymer electrolytes system due to its good conduction properties since it has the anionic site (COO^-), which is susceptible to the NH_4^+ or any cations. These cations can trigger more interactions to take place; thus it is possible to enhance the conduction properties. The transporting of protons in this work could be attributed to the NH_4^+ component, either H^+, NH_3 or NH_4^+ [61, 62].

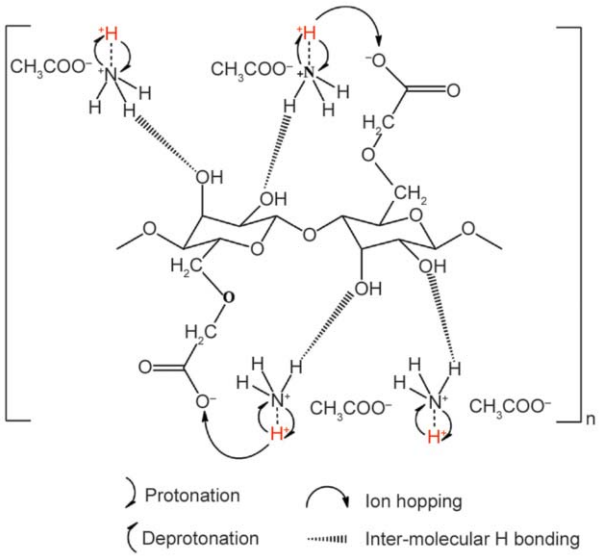

Figure 4. Schematic diagram of CMC having interacted with $NH_4CH_3CO_2$ via [NH_3–H^+].

3.2. X-ray diffraction analysis

Figure 5a shows the XRD patterns of the CMC doped with $NH_4CH_3CO_2$, which gave a broad peak between the region of 11.04 and 34.20°. The intensity of this broad peak decreased with the addition of 5 to 15 wt% of $NH_4CH_3CO_2$. This might be influenced by the complexation between CMC and $NH_4CH_3CO_2$ in the present system as previously discussed in the FTIR analysis. During the process of protonation and deprotonation of H–$^+NH_4CH_3CO_2$, the arrangement of the CMC polymer chain became more disorderly due to the occurrence of complexation. This was attributed to the increase in the amorphous phase which would influence the ionic conductivity of the BPEs system as suggested in the previous studies conducted by Kamarudin and Isa [63] and Samsudin *et al*. [64]. However, upon further addition of 20 to 25 wt% of $NH_4CH_3CO_2$, the peaks became more intensified, suggesting the re-formation of crystalline structure. This finding is in agreement with Selvalakshmi *et al*. [65], who mentioned the re-association of ammonium salt that leads to significant loss in the number of mobile ions.

The XRD deconvolution technique is adopted to study the amorphous nature in the BPEs system. The XRD deconvolution of the CMC-$NH_4CH_3CO_2$ BPEs is shown in Figure 5b. As depicted in the figure, the amorphous peaks are shown by dot-dashed line while the crystalline peaks are shown by the solid black line. The results of the deconvolution study were quite similar to those of previous studies [66, 67]. The degree of crystallinity of BPEs was calculated by using the Equation (5). From that equation, it was determined that the degree of crystallinity is inversely proportional to the amorphous value. The amorphous phase is more favorable to the enhancement of ionic conductivity.

The calculated percentage crystallinity of the CMC-$NH_4CH_3CO_2$ BPEs system is presented in the inset value in Figure 5b. It can be noted here that the samples with smaller crystallite size and more amorphous behavior exhibited higher ionic conductivity [68]. It was observed that the addition of 0 to 10 wt% of $NH_4CH_3CO_2$ to CMC caused a decrease in the percentage of crystallinity, which in turn increased

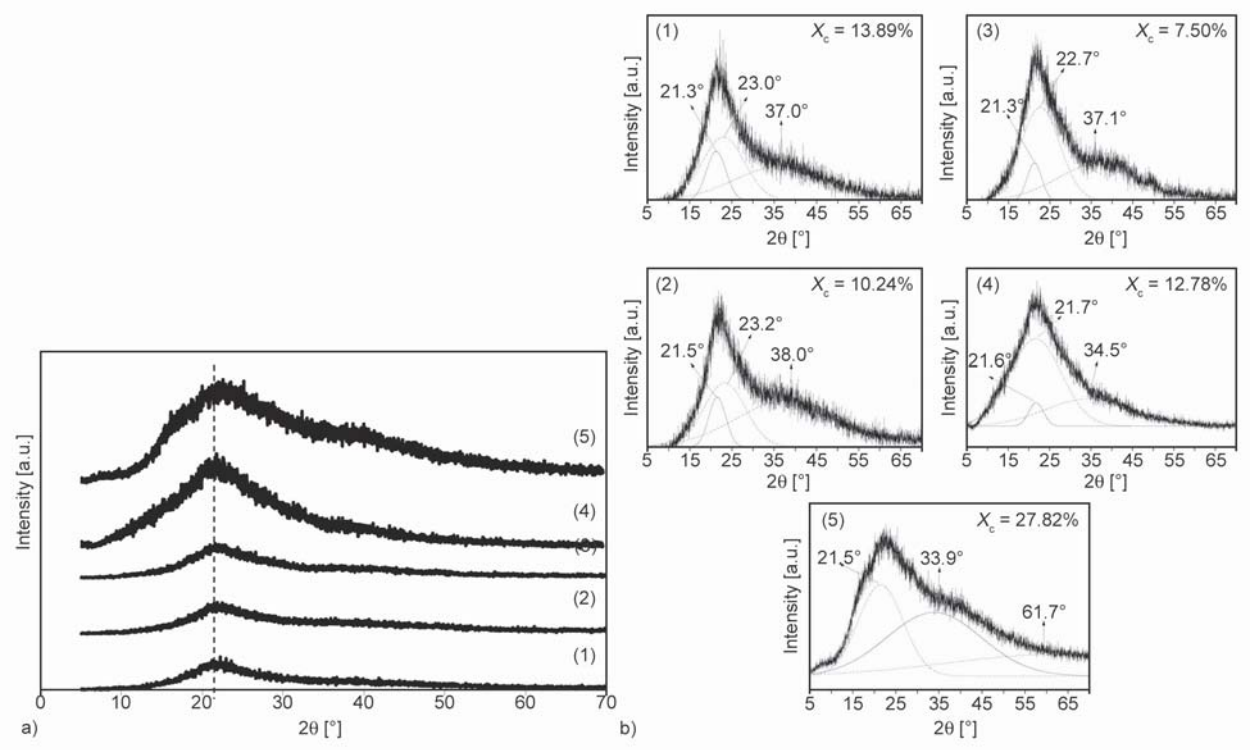

Figure 5. XRD analysis of sample (1) 1, (2) 2, (3) 3, (4) 5 and (5) 6 of CMC-$NH_4CH_3CO_2$ BPEs system (a) XRD spectra and (b) XRD deconvolution.

the amorphousness of this BPEs system. This increased amorphousness promoted the transportation of ions and increased the ionic conductivity of the BPEs system [39]. The FTIR analysis also supported this observation where the addition of ammonium salt caused complexation to occur and hence increased the flexibility of the polymer chain's segmental motion. This is primarily due to the contribution of the increased protonation (H^+) in the amorphous state in the CMC-$NH_4CH_3CO_2$ BPEs system. Hence, the sample that contained 10 wt% was expected to exhibit the highest ionic conductivity since it had the largest amorphous domain and conversely, lowest crystallinity.

3.3. Ionic conduction analysis

A Nyquist plot of the various samples of the CMC-$NH_4CH_3CO_2$ BPEs system at ambient conditions is presented in Figure 6. The plot shows an incomplete or compressed semicircle curve. The semi-circular curves appeared at a higher frequency (left towards origin), whereas an inclined straight line to the semicircular curve was located at the lower-frequency region. Previous studies that used impedance analysis to characterize polymer electrolytes showed that Nyquist plots containing a semicircle were due to a parallel combination of bulk resistance, R_b, and bulk capacitance, C_b, of the present electrolyte system [69, 70]. However, we noted that the semicircle was

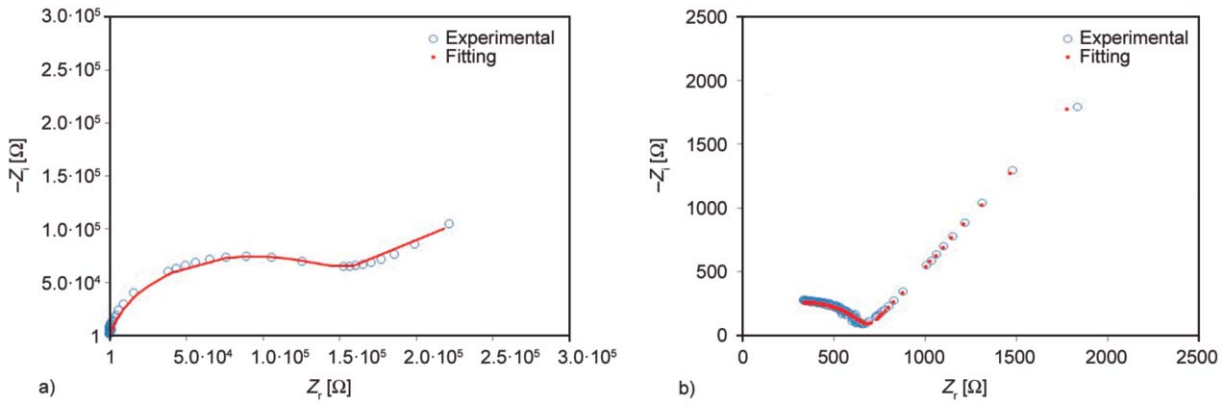

Figure 6. Fitting analysis for sample (a) 1 and (b) 3, of the CMC-$NH_4CH_3CO_2$ BPEs system.

reduced, which could be attributed to the complexation that altered the structural properties of the BPEs as proven by the FTIR and XRD analyses. Notably, Figure 6b shows a tilted semicircle and inclined spike, elucidating that the system has experienced an increase of ionic mobility and also number of ion carriers [53].

The physical origin of the *CPE* was the non-conducting crystalline regions linked with the conducting amorphous phase within the space in the BPEs system. This was due to the movement of the ions in the bulk of the sample and also different relaxation times [71, 72]. The fact that the appearance of the semicircle was placed below the real part (Z_r), discloses the non-Debye behavior of the present sample and the intercept of the semicircle with the Z_r provided the R_b value which can be calculated by using the Equation (10) [73, 74]:

$$R_b = \frac{1}{\omega C_b} \tag{10}$$

where ω is angular frequency and C_b is bulk capacitance.

In this present work, the inclined straight lines (spike) to the semicircle which were found in all samples were mainly attributed to the electrode polarization effect that represents the diffusion activity [75]. It was shown that the spike for the Nyquist plot was inclined at an angle lower than 90° with the Z_r axis. This could be due to the inhomogeneous distribution or irregularity of the electrode-electrolyte interface of the BPEs system when $NH_4CH_3CO_2$ was added [76]. The spike can be assigned with CPE_2, and the fitted circuit can be described by a parallel arrangement of R_b and CPE_1 together with another CPE_2 in a series, as shown in Figure 7. The impedance of *CPE* element (Z_{CPE}) can be defined as shown by Equations (11) and (12) [77]:

$$Z_{CPE} = \frac{1}{k(j\omega)^p} \text{ where } 0 \le p \le 1 \tag{11}$$

or

$$Z_{CPE} = \frac{k\left(\cos\frac{p\pi}{2} + j\sin\frac{p\pi}{2}\right)}{\omega p} \tag{12}$$

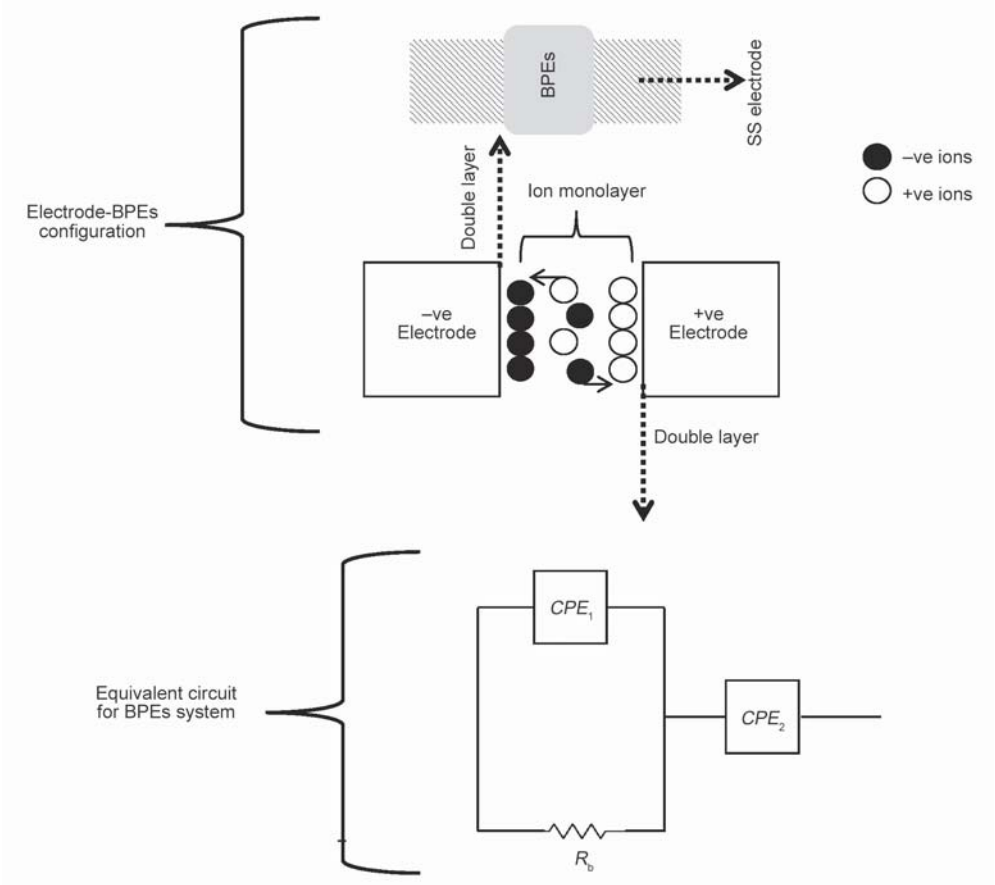

Figure 7. Schematic diagram of the electrode-electrolytes interaction of BPEs system and its equivalent circuit.

Here ω is angular frequency (ω = 2π*f*, where *f* is frequency), k^{-1} corresponds to the capacitance value of the *CPE* element and *p* is the deviation from the vertical axis in the Z_i *versus* Z_r plot. The values of Z_i and Z_r associated with the fitted circuit were adopted from Bandara and Mellander, see Equations (13) and (14) [78]:

$$Z_r = \frac{R_b + R_b^2 k_1^{-1} \omega^{p_1} \cos\frac{\pi p_1}{2}}{1 + 2R_b k_1^{-1} \omega^{p_1} \cos\frac{\pi p_1}{2} + R_b^2 k_1^{-2} \omega^{2p_1}} + \frac{\cos\frac{\pi p2}{2}}{k_2^{-1} \omega p_2} \quad (13)$$

$$Z_i = \frac{R_b^2 k_1^{-1} \omega^{p_1} \sin\frac{\pi p_1}{2}}{1 + 2R_b k_1^{-1} \omega p_1 \cos\frac{\pi p_1}{2} + R_b^2 k_1^{-2} \omega^{2p_1}} + \frac{\cos\frac{\pi p2}{2}}{k_2^{-1} \omega p_2} \quad (14)$$

It was found that the appearance of the semicircle at higher frequencies was reduced in the BPEs system with an increment of up to 10 wt% $NH_4CH_3CO_2$. This suggested that only the resistive component of the BPEs system was shown. With the addition of higher composition of $NH_4CH_3CO_2$ (more than 10 wt%), the semicircle re-emerged. The reappearance of the semicircle at the higher $NH_4CH_3CO_2$ composition was due to the overcrowding of $NH_4CH_3CO_2$ that lead to the aggregation of the ions and decreased the charge carrier process. This caused the ionic conductivity of the electrolytes system to be affected as expected.

Table 1 shows the fitting parameters involved in the equivalent circuit. The parameters attained from the fitting analysis are comparable to those reported from other works [75, 79].

The determination of the optimum ionic conductivity in the present system can be considered as one type of solid polymer electrolytes (SPEs), where the ionic conductivity values fell in the range of 10^{-2} to 10^{-6} S/cm as reported by other studies [46, 61–65].

Table 1. The parameter of the circuit element for BPEs system at ambient temperature (303 K).

Sample	R_b [Ω]	p_1 [rad]	CPE_1 [F]	p_2 [rad]	CPE_2 [F]
1	152900	0.880	4.18×10^{-9}	0.770	7.91×10^{-6}
2	2000	0.790	4.38×10^{-8}	0.621	1.32×10^{-6}
3	665	0.825	2.52×10^{-8}	0.644	5.46×10^{-5}
4	11550	0.850	6.70×10^{-8}	0.725	1.46×10^{-6}
5	37365	0.850	6.79×10^{-8}	0.700	3.10×10^{-6}
6	52876	0.837	1.49×10^{-8}	0.330	$6.90\ 10^{-6}$

The variation in ionic conductivity, σ, with the $NH_4CH_3CO_2$ composition of the BPEs system at room temperature, is illustrated in Figure 8. Based on the figure, the conductivity of pure CMC was rather low, which was attributed to the conjugated double bond at the carboxylate anion in the structure of the CMC. The presence of this conjugation provides charges through electronic delocalization of the backbone [80]. In addition, the flexibility of the polymer backbone is also regarded as another factor that can improve conductivity. This can be correlated to the amorphous properties of the CMC which was discussed previously in the XRD analysis. However, the ionic conductivity rose with the introduction of $NH_4CH_3CO_2$ and achieved the maximum value of 5.07×10^{-6} S/cm for sample 3 which contained 10 wt% of $NH_4CH_3CO_2$.

In this present work, the increase in ionic conductivity due to increased wt% of $NH_4CH_3CO_2$ aligned with the decrease of the bulk resistance value as observed in the Nyquist plot fitting. This can be linked to the increasing ionic mobility and the number of ions of the BPEs system [64, 75]. Moreover, it is also due to the increasingly amorphous phase of the CMC-$NH_4CH_3CO_2$ BPEs system as observed in the XRD spectra analysis. As the amorphous phase progressively increased, faster segmental motion was induced in the host polymer and favored inter– or intrachain ion hopping from one site to another site and affected the ionic conductivity.

Apparently, the addition of 15 wt% until the composition of 25 wt% of $NH_4CH_3CO_2$, has led to a decrement in ionic conductivity. The addition of $NH_4CH_3CO_2$ above the optimum composition caused a decrease in ionic conductivity due to the

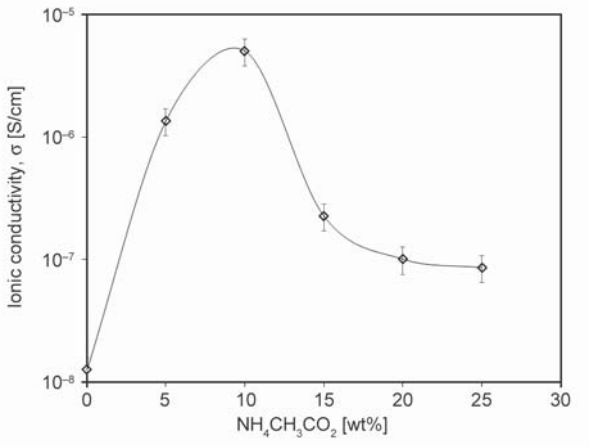

Figure 8. Ionic conductivity against $NH_4CH_3CO_2$ [wt%] at room temperature.

bio-polymer host matrix (CMC) becoming saturated, and subsequently reducing the number of charges, therefore, limiting its mobility in the BPEs system [81]. The theoretical impedance analysis also supported the results where the conductivity decreased with the appearance of the semicircle in the BPEs system. As the segmental polymer chain becomes limited, the movement of ions and the conductivity of the BPEs accordingly become lower.

Table 2 shows a comparison of ionic conductivity values obtained from the literature for single polymers and polymer blend electrolytes derived from natural and synthetic polymers. The ionic conductivity for various types of solid polymer electrolytes that were reported in the literature fell within the ~10^{-6} to ~10^{-9} S/cm range. Nevertheless, the optimum ionic conductivity for the BPEs in the present work is comparable with those in the literature, even though it was derived from a single polymer. Consequently, this result is regarded as a pilot result which offers greater prospect for the use of CMC doped with $NH_4CH_3CO_2$ for the next generation of electrochemical devices.

In this present work, the dependence of ionic conductivity on temperature was analyzed to understand the conduction mechanism in the CMC-$NH_4CH_3CO_2$ BPEs system. Figure 9 shows the ionic conductivity of the CMC-$NH_4CH_3CO_2$ BPEs system at different temperatures. The ionic conductivity of the CMC-$NH_4CH_3CO_2$ BPEs increased with increasing temperature where there was no sudden drop in the conductivity value. This indicated that no phase transition occurred in the biopolymer matrix nor domains formed with the addition of $NH_4CH_3CO_2$ [82]. As a result, it was proven that the CMC-$NH_4CH_3CO_2$ BPEs obeys the Arrhenius rule, *i.e.*, conduction is a thermally activated process as reported by other researchers [64, 66, 83, 84].

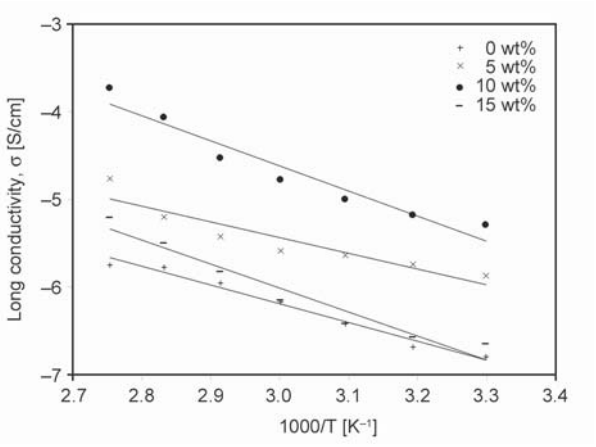

Figure 9. Temperature dependence for CMC-$NH_4CH_3CO_2$ BPEs system.

Furthermore, a higher temperature provides more energy to overcome the energy barrier between the sites during the migration of H^+ towards the CMC, and this can be seen in the sample containing 20 wt% of $NH_4CH_3CO_2$. Other than that, based on studies conducted by Kamarudin *et al*. [84] and Hema *et al*. [85], the ionic conductivity increase with increasing temperature is due to the increase in permitted volume which is related to the segmental (polymer chain) motion. This increasing polymer free volume facilitates the translational ionic motions, which in turn, favor intra-chain and inter-chain movements in the CMC-$NH_4CH_3CO_2$ BPEs system and resulting in higher ionic conductivity as the temperature increases [46, 81]. Based on the temperature dependence plot, the activation energy was calculated using the Arrhenius relationship equation [70–74], and the highest conductivity had the lowest activation energy of 0.24 eV. Our finding is comparable with Bakar *et al*.

Table 2. Comparison of the CMC-$NH_4CH_3CO_2$ BPEs ionic conductivity with other synthetic and bio-polymer electrolyte systems from the literature.

Polymer host	Ionic dopant	Ionic conductivity, σ [S/cm]	Reference
Sago	NH_4Br	6.90×10^{-9}	[71]
Carrageenan	NaOH	5.30×10^{-7}	[72]
Gelatin	CH_3COOH	1.28×10^{-5}	[73]
Chitosan	$Eu(Trif)_3$	1.52×10^{-6}	[74]
Pectin	NH_4SCN	4.05×10^{-6}	[12]
Polyurethanes	LiCl	9.20×10^{-8}	[75]
Polyethylene oxide	$LiAsF_6$	1.58×10^{-7}	[5]
Polyethylene oxide/Polyvinyl pyrrolidone	$NaIO_4$	1.56×10^{-7}	[76]
Chitosan/Polyethylene oxide	NH_4I	3.66×10^{-6}	[77]
CMC	$NH_4CH_3CO_2$	~10^{-6}	Present system

[86], who worked on an eco-friendly CMC-chitosan bio-polymer doped with dodecyltrimethylammonium bromide (DTAB) where they reported the highest conducting sample (~10^{-6} S/cm) in their work gave the activation energy value of 0.33 eV.

3.4. Transport properties analysis

The FTIR spectra of the selected region were deconvoluted and then plotted in Figure 9. The highlighted peak is in the range of 1500 to 1700 cm^{-1} which corresponded to the COO^- of CMC, and this was due to the significant complexation that occurred between CMC-$NH_4CH_3CO_2$ as suggested by the FTIR analysis. The free ions and contact ions that were observed in Figure 10 were tabulated in Table 3. The free ions can be assigned in the middle of the three peaks while the contact ions can be assigned to free ions [6, 38, 40]. It was found that the percentage of free ions increased upon the addition of $NH_4CH_3CO_2$. This was primarily due to the increment of H^+ ion dissociation from NH_4^+ that allowed sufficient ion passage and in turn, boosted the ionic conductivity as discussed earlier and in agreement with the peak observed in the FTIR analysis. The transport properties of the present system are presented in Figure 11.

Based on Figure 11a, it can be seen clearly that the η values increased linearly by the addition of $NH_4CH_3CO_2$. The number of ions (η) is mainly linked to the changes in concentration of free ions [87]. The value of μ and *D* for samples 2 and 3 show increasing trend which is parallel with the conductivity trend. Thus, these results clearly revealed that the mobility of ions (μ) and the diffusion coefficient (*D*) [83, 88] contributed to the ionic conductivity, as they contributed to the dissociation of free ions in BPEs system

Table 3. Free ions and contact ions of the CMC-$NH_4CH_3CO_2$ BPEs system.

Sample	Free ions [%]	Contact ions [%]
1	n.a	n.a
2	61.33	38.67
3	65.54	34.46
4	64.70	35.30

n.a = not available

as shown in Figure 11b. In general, the ionic conductivity is linked with the equation $\sigma = \eta \cdot q \cdot \mu$ [41, 83]. Based on the equation, the transport parameter is influenced greatly by the ionic conductivity value. This leads to the increment of transport properties into maximum value. Furthermore, the pattern of η increased linearly with the addition of $NH_4CH_3CO_2$ due to the overcrowding of protons as ammonium ions (NH_4^+), so that more energy was required to break away to allow for ions migration. As ions encounter difficulty in migration in the CMC-$NH_4CH_3CO_2$, therefore there was a decrement in μ, *D* and also ionic conductivity.

Figure 11c shows the $NH_4CH_3CO_2$ composition dependence of the diffusion coefficient for ammonium ions including H^+ by MD calculation. The diffusion coefficient exhibited the maximum value at 10 wt% $NH_4CH_3CO_2$ and the curve trend matched well with the results from the experimental work as shown in Figure 11b. The results of the MD calculation indicated that the CMC was protonated by $NH_4CH_3CO_2$ via inter- or intramolecular hydrogen bonds, as proposed in Figure 4, which enhanced the amorphousness of the entire system and provided more pathways for the movement of H^+. This observation was also supported by the FTIR and XRD analyses that were discussed in the preceding section. The amorphous phase

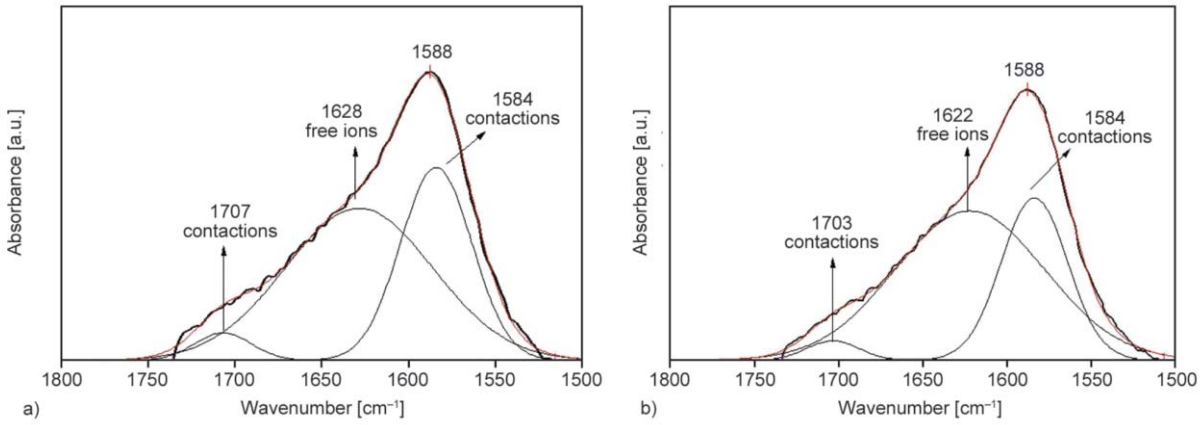

Figure 10. FTIR deconvolution of sample (a) 2 and (b) 3 of the CMC-$NH_4CH_3CO_2$ BPEs system.

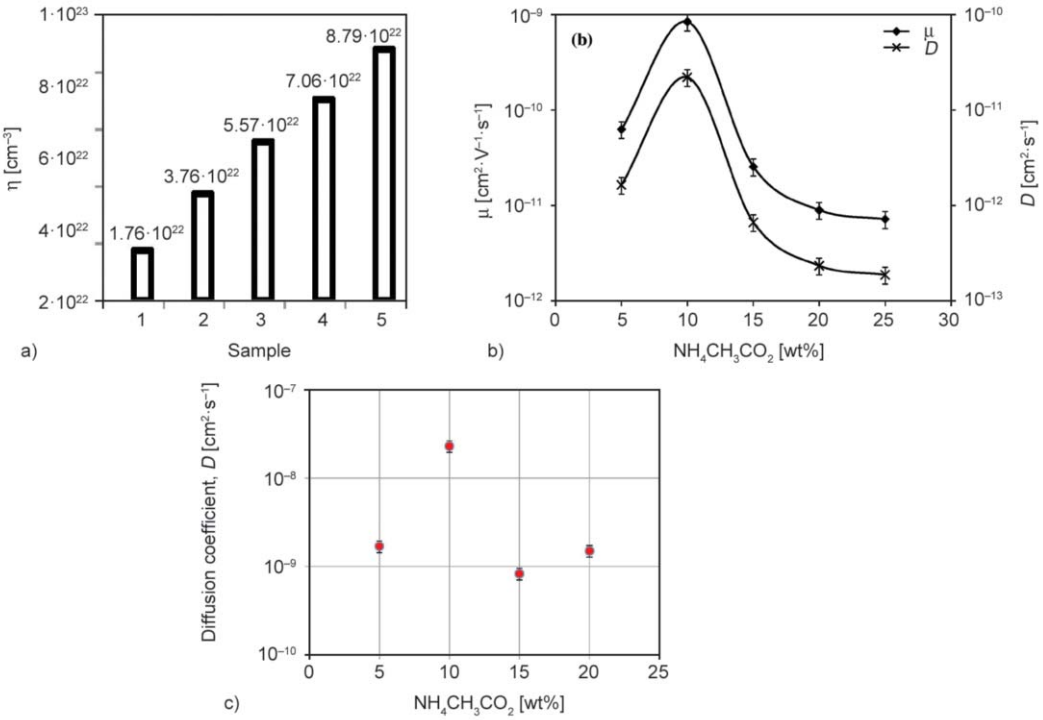

Figure 11. Transport parameters (a) number, η and (b) mobility, μ, and diffusion coefficient (*D*) of ions and (c) diffusion coefficient (*D*) by MD calculation of CMC-$NH_4CH_3CO_2$ BPEs system.

allowed more ions to transport within the biopolymer-salt complex systems and hence increased the ionic conductivity.

3.5. Transference number measurement (TNM)

In order to identify the conducting species in the electrolytes, the transference number measurements were carried out. By sandwiching the electrolyte with the conducting species transparent electrodes, a transference number of the conducting species can be known from the ratio of steady-state current to the initial current (I_{ss}/I_i). To determine the transference number of electron (t_e), stainless steel electrodes were used since electrons are transparent to the ion blocking stainless steel [89]. For ionic conductors, the current flowing through the electrode falls rapidly with time, while for non-ionic conductors, the current would not decrease with time [90]. The plot of polarization current against time for our highest conducting sample (sample 3) is shown in Figure 12. The current was observed to fall rapidly at the initial, before being saturated to a lower current value. This phenomenon indicated that the polymer electrolytes are ionic conductors. By knowing the electron transference number, t_e, the value of the ionic transference number, t_{ion} of the BPEs system was calculated based on the literature [91].

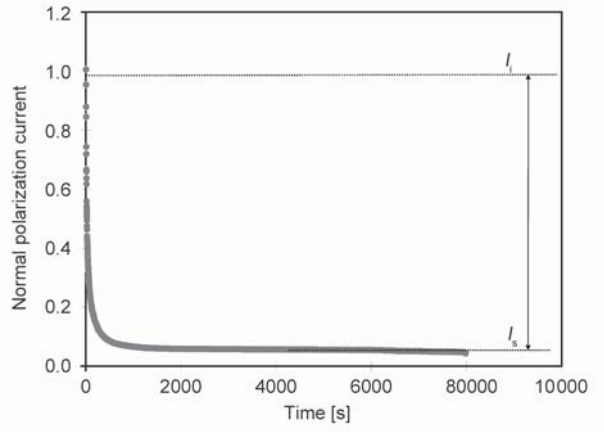

Figure 12. TNM plot for sample 3.

The t_{ion} and t_e of the highest ionic conductivity (sample 3) studied were found to be 0.97 and 0.03 respectively. These results clearly revealed that the $NH_4CH_3CO_2$ complexed with the CMC BPEs system which involved ions transport as discussed previously in the FTIR and transport properties analyses. Thus, it can be inferred that the conducting charge species in the sample was predominantly due to ions since the t_{ion} measured was ~1 which is in agreement with other research work [47, 92].

3.6. Voltammetry analysis

The electrochemical stability (*i.e*. working cell potential range) of polymer electrolytes is an important parameter to be evaluated for their potential application in electrochemical devices. The stability window of the BPEs system for sample 3 was studied using the linear sweep voltammetry (LSV) technique, and its corresponding voltammogram is shown in Figure 13. It can be observed that there was no current through the working electrode from the open circuit potential of 1.72±0.01 V as shown in Figure 13. This corresponded to the plating of sample 3 onto the stainless steel electrode and may be related to the decomposition of the sample. The result showed that the current increased significantly when the potential was higher than 1.72 V which indicated the decomposition of the present electrolyte system. Kadir *et al*. [93] reported that the decomposition voltage of plasticized methylcellulose – NH_4Br polymer electrolyte is 1.53 V, and the electrolyte was used in the fabrication of an electrical double-layer capacitor (EDLC). The present result showed that sample 3 which was the highest conducting electrolyte in the present work could be used for the fabrication of an EDLC.

3.7. Electrical double layer capacitor (EDLC) analysis

In the present work, a cyclic voltammetry (CV) measurement was conducted to evaluate the possibility of using our BPEs system (sample 3) as an EDLC. Figure 14 shows the CV plot of the EDLC at various scan rates. As shown in the figure, no peaks were observed in the plot, indicating that no redox reactions occurred in the potential range of 0 to 1 V. This EDLC behavior was also observed by other researchers [94–96]. The shape of the plot changed to a nearly rectangular shape as the scan rate decreased. Meanwhile, higher scan rates showed the inconsistency of the CV shape from the perfect rectangular shape, which can be attributed to the carbon porosity of active materials and the internal resistance, thus creating a current dependence of voltage [97, 98]. Based on the CV plot, the specific capacitances (C_s) were calculated using Equation (9) and were plotted as shown in the inset of Figure 14. The value of C_s increased as the scan rate decreased with the highest value of C_s being ~2.7 F/g for the scan rate of 2 mV/s. The optimum C_s value at lower scan rate could be due to the ions having enough time to diffuse and utilize all of the vacant sites in the active electrode material since the mobility was higher as shown by the transport properties analysis.

Galvanostatic charge–discharge (GCD) cycling was carried out in the potential range between 0 and 1 V as shown in Figure 15a. The charge–discharge characteristic was tested at different current (0.05, 0.03 and 0.02 mA). From the graph, it can be observed that the values of $I_{R\ drop}$ increased with increasing applied current during the charge-discharge cycle. This observation can be related to the Ohm's law equation; $V_{cell} = Voc - I_{R\ cell}$, where V_{oc} is maximum voltage when the circuit is open and R is the resistance of the EDLC. From the equation, the voltage of the cell is proportional to the current and resistance values. Therefore, it is important to reduce the resistance of the EDLC cell to minimize the $I_{R\ drop}$.

Figure 15b shows the specific capacitance, ESR and coulombic efficiency of the EDLC above the 300th cycles which operated using current of 0.02 mA. A theoretical estimate of a single electrode capacitance

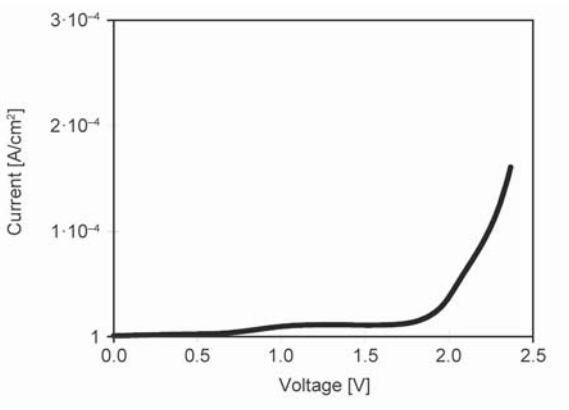

Figure 13. LSV plot for sample 3.

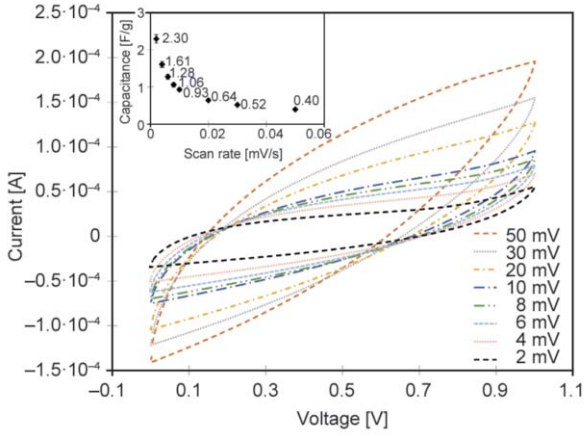

Figure 14. Cyclic voltammograms of EDLC at different scan rates.

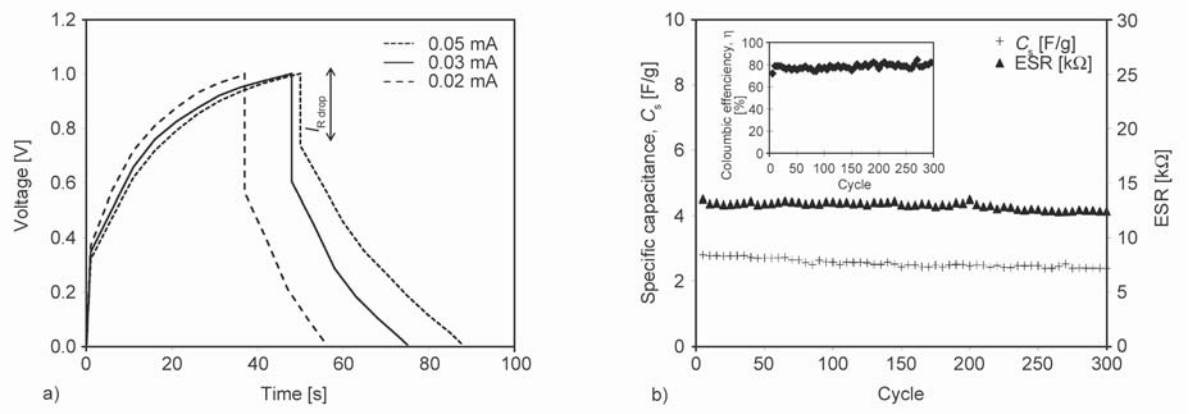

Figure 15. (a) Charge-discharge curves of EDLC at different applied current and (b) their characteristics at different cycle.

using AC as active materials is ~400 F/g for a total surface area of 2000 m^2/g [99]. However, the present EDLC gave the specific capacitance of 2.8 F/g at the 5th cycles and 2.4 F/g at the 300th cycles with a coulombic efficiency of ~80%. This value was quite similar to the value observed from the CV analysis with a scan rate 2 mV. The difference between the theoretical and experimental values of C_s can be attributed to the inability of the present electrolytes to take maximum advantage of the activated carbon electrodes total surface area in producing a large double-layer capacitance. It was found that the calculated value of ESR was in the range of 12~13 kΩ of the EDLC measured until the 300th cycles. According to Arof *et al.* [100], the higher values of ESR may be related to the low cation transference number, degradation and low ionic conductivity of the present electrolytes system. Taking into account the average specific capacitance of ~3 F/g and even lower C_s value, the EDLC that employs a proton-conducting biopolymer electrolyte based on the CMC-$NH_4CH_3CO_2$ can be further exploited to enhance its performance.

4. Conclusions

In this present work, a series of new biopolymer electrolytes (BPEs) based on the CMC-$NH_4CH_3CO_2$ were successfully prepared via the solution casting technique. The FTIR analysis revealed the interaction of CMC with the increasingly added $NH_4CH_3CO_2$, suggesting that there is a strong affinity between the H^+ of the $NH_4CH_3CO_2$ with the C–O–C (1063 cm^{-1}) and COO^- (1597 cm^{-1}) groups in the CMC due to the inter- and intra-molecular attraction. The XRD analysis confirmed that the optimum ionic conductivity at ambient temperature for the BPEs system was achieved by the most amorphous sample that contained 10 wt% of $NH_4CH_3CO_2$ with a value of 5.07×10^{-6} S·cm^{-1}. The trend in ionic conductivity for the CMC-$NH_4CH_3CO_2$ BPEs system was governed by the ions mobility and diffusion coefficient properties as proven by the MD calculation and imitated a similar trend of free ions. Meanwhile, the number of mobile ions increased slightly with the addition of $NH_4CH_3CO_2$ as revealed by the deconvolution analysis. The significance of the dielectric and modulus study was emphasized to comprehend the proton conduction mechanism in the BPEs system. Towards the application of the present BPEs in an EDLC, the LSV of the highest conducting sample revealed the highest electrochemical window of 1.72 V and gave a specific capacitance value of ~2.4 F/g. The process efficiency was sustained at ~80% for up to 300th cycles which suggests that this BPEs system can be an excellent alternative solid-state system for further application in electrochemical devices.

Acknowledgements

The authors would like to thank the Ministry of Higher Education Malaysia for FRGS grant (RDU1901114) and FIST UMP for the technical and research support.

References

[1] Armand M. B.: Polymer electrolytes. Annual Review of Materials Science, **16**, 245–261 (1986). https://doi.org/10.1146/annurev.ms.16.080186.001333

[2] Itoh T., Nakamura K., Uno T., Kubo M.: Thermal and electrochemical properties of poly(2,2-dimethoxypropylene carbonate)-based solid polymer electrolyte for polymer battery. Solid State Ionics, **317**, 69–75 (2018). https://doi.org/10.1016/j.ssi.2017.12.030

[3] Jabbour L., Bongiovanni R., Chaussy D., Gerbaldi C., Beneventi D.: Cellulose-based Li-ion batteries: A review. Cellulose, **20**, 1523–1545 (2013). https://doi.org/10.1007/s10570-013-9973-8

[4] Yahya M. A. Z., Harun M. K., Ali A. M. M., Mohammat M. F., Hanafiah M. A. K. M., Ibrahim S. C., Mustaffa M., Darus Z. M., Latif F.: XRD and surface morphology studies on chitosan-based film electrolytes. Journal of Applied Sciences, **6**, 3150–3154 (2006). https://doi.org/10.3923/jas.2006.3150.3154

[5] Yan X., Peng B., Hu B., Chen Q.: PEO-urea-LiTFSI ternary complex as solid polymer electrolytes. Polymer, **99**, 44–48 (2016). https://doi.org/10.1016/j.polymer.2016.06.056

[6] Zainuddin N. K., Samsudin A. S.: Investigation on the effect of NH_4Br at transport properties in k–carrageenan based biopolymer electrolytes via structural and electrical analysis. Materials Today Communications, **14**, 199–209 (2018). https://doi.org/10.1016/j.mtcomm.2018.01.004

[7] Aihara Y., Appetecchi G., Scrosati B., Hayamizu K.: Investigation of the ionic conduction mechanism of composite poly(ethyleneoxide) PEO-based polymer gel electrolytes including nano-size SiO_2. Physical Chemistry Chemical Physics, **4**, 3443–3447 (2002). https://doi.org/10.1039/B201991B

[8] Sun B., Mindemark J., Edström K., Brandell D.: Polycarbonate-based solid polymer electrolytes for Li-ion batteries. Solid State Ionics, **262**, 738–742 (2014). https://doi.org/10.1016/j.ssi.2013.08.014

[9] Ramesh S., Liew C-W., Morris E., Durairaj R.: Effect of PVC on ionic conductivity, crystallographic structural, morphological and thermal characterizations in PMMA–PVC blend-based polymer electrolytes. Thermochimica Acta, **511**, 140–146 (2010). https://doi.org/10.1016/j.tca.2010.08.005

[10] Shim J., Kim L., Kim H. J., Jeong D., Lee J. H., Lee J-C.: All-solid-state lithium metal battery with solid polymer electrolytes based on polysiloxane crosslinked by modified natural gallic acid. Polymer, **122**, 222–231 (2017). https://doi.org/10.1016/j.polymer.2017.06.074

[11] Singh R., Bhattacharya B., Tomar S. K., Singh V., Singh P. K.: Electrical, optical and electrophotochemical studies on agarose based biopolymer electrolyte towards dye sensitized solar cell application. Measurement, **102**, 214–219 (2017). https://doi.org/10.1016/j.measurement.2017.02.014

[12] Vahini M., Muthuvinayagam M.: AC impedance studies on proton conducting biopolymer electrolytes based on pectin. Materials Letters, **218**, 197–200 (2018). https://doi.org/10.1016/j.matlet.2018.02.011

[13] Alves R., Sentanin F., Sabadini R. C., Fernandes M., de Zea Bermudez V., Pawlicka A., Silva M. M.: Samarium (III) triflate-doped chitosan electrolyte for solid state electrochromic devices. Electrochimica Acta, **267**, 51–62 (2018). https://doi.org/10.1016/j.electacta.2018.02.044

[14] Nawaz H., Casarano R., El Seoud O. A.: First report on the kinetics of the uncatalyzed esterification of cellulose under homogeneous reaction conditions: A rationale for the effect of carboxylic acid anhydride chain-length on the degree of biopolymer substitution. Cellulose, **19**, 199–207 (2012). https://doi.org/10.1007/s10570-011-9622-z

[15] Bayer T., Cunning B. V., Selyanchyn R., Nishihara M., Fujikawa S., Sasaki K., Lyth S. M.: High temperature proton conduction in nanocellulose membranes: Paper fuel cells. Chemistry of Materials, **28**, 4805–4814 (2016). https://doi.org/10.1021/acs.chemmater.6b01990

[16] Wang Y., Liu L., Chen P., Zhang L., Lu A.: Cationic hydrophobicity promotes dissolution of cellulose in aqueous basic solution by freezing–thawing. Physical Chemistry Chemical Physics, **20**, 14223–14233 (2018). https://doi.org/10.1039/C8CP01268G

[17] Zecher D., Gerrish T.: Cellulose derivatives. Thickening and gelling agents for food. Springer, Dordrecht (1997). https://doi.org/10.1007/978-1-4615-2197-6_4

[18] Azizi Samir M. A. S., Alloin F., Dufresne A.: Review of recent research into cellulosic whiskers, their properties and their application in nanocomposite field. Biomacromolecules, **6**, 612–626 (2005). https://doi.org/10.1021/bm0493685

[19] Huang J., Dufresne A., Lin N.: Nanocellulose: From fundamentals to advanced materials. Wiley, Weinheim (2019).

[20] Sindhu K., Prasanth R., Thakur V. K.: Medical applications of cellulose and its derivatives: Present and future. in 'Nanocellulose polymer nanocomposites: Fundamentals and applications. (ed.: Thakur V. K.) Wiley, Hoboken, Vol 14, 437–477 (2014). https://doi.org/10.1002/9781118872246.ch16

[21] Timhadjelt L., Serier A., Boumerdassi K., Serier M., Aîssani Z.: Modification of cellulose for an application in the waste water treatment. in 'Damage and fracture mechanics' (eds.: Boukharouba T., Elboujdaini M., Pluvinage G.) Springer, Dordrecht 531–538 (2009) https://doi.org/10.1007/978-90-481-2669-9_56

[22] Wüstenberg T.: Cellulose and cellulose derivatives in the food industry. Wiley Weinheim (2014). http://doi.org/10.1002/9783527682935

[23] Trache D., Hussin M. H., Haafiz M. M., Thakur V. K.: Recent progress in cellulose nanocrystals: Sources and production. Nanoscale, **9**, 1763–1786 (2017). https://doi.org/10.1039/C6NR09494E

[24] Bella F., Chiappone A., Nair J. R., Meligrana G., Gerbaldi C.: Effect of different green cellulosic matrices on the performance of polymeric dye-sensitized solar cells. Chemical Engineering Transactions, **41**, 211–216 (2014). https://doi.org/10.3303/CET1441036

[25] Bella F., Galliano S., Falco M., Viscardi G., Barolo C., Grätzel M., Gerbaldi C.: Approaching truly sustainable solar cells by the use of water and cellulose derivatives. Green Chemistry, **19**, 1043–1051 (2017). https://doi.org/10.1039/C6GC02625G

[26] Gupta P. K., Raghunath S. S., Prasanna D. V., Venkat P., Shree V., Chithananthan C., Choudhary S., Surender K., Geetha K.: An update on overview of cellulose, its structure and applications. IntechOpen, Rijeka (2019). https://doi.org/10.5772/intechopen.84727

[27] Ahmad N. H. B., Isa M. I. N. B. M.: Proton conducting solid polymer electrolytes based carboxymethyl cellulose doped ammonium chloride: ionic conductivity and transport studies. International Journal of Plastics Technology, **19**, 47–55 (2015). https://doi.org/10.1007/s12588-015-9110-7

[28] Samsudin A. S., Isa M. I. N.: Structural and electrical properties of carboxy methylcellulose-dodecyltrimethyl ammonium bromide-based biopolymer electrolytes system. International Journal of Polymeric Materials, **61**, 30–40 (2012). https://doi.org/10.1080/00914037.2011.557810

[29] Noor N. A. M., Isa M. I. N.: Ionic conductivity and dielectric properties of CMC doped NH_4SCN solid biopolymer electrolytes. **1107**, 230–235 (2016). https://doi.org/10.4028/www.scientific.net/AMR.1107.230

[30] Chai M., Isa M. I. N.: Carboxyl methylcellulose solid polymer electrolytes: Ionic conductivity and dielectric study. Journal of Current Engineering Research, **1**, 23–27 (2011).

[31] Yokota S., Ueno T., Kitaoka T., Wariishi H.: Molecular imaging of single cellulose chains aligned on a highly oriented pyrolytic graphite surface. Carbohydrate Research, **342**, 2593–2598 (2007). https://doi.org/10.1016/j.carres.2007.08.018

[32] Aziz S. B., Hamsan M. H., Brza M. A., Kadir M. F. Z., Abdulwahid R. T., Ghareeb H. O., Woo H. J.: Fabrication of energy storage EDLC device based on CS:PEO polymer blend electrolytes with high Li^+ ion transference number. Results in Physics, **15**, 102584/1–102584/13 (2019). https://doi.org/10.1016/j.rinp.2019.102584

[33] Aziz S. B., Hamsan M. H., Abdullah R. M., Kadir M. F. Z.: A promising polymer blend electrolytes based on chitosan: Methyl cellulose for EDLC application with high specific capacitance and energy density. Molecules, **24**, 2503/1–2503/24 (2019). https://doi.org/10.3390/molecules24132503

[34] Zhu Y. S., Xiao S. Y., Li M. X., Chang Z., Wang F. X., Gao J., Wu Y. P.: Natural macromolecule based carboxymethyl cellulose as a gel polymer electrolyte with adjustable porosity for lithium ion batteries. Journal of Power Sources, **288,** 368–375 (2015). https://doi.org/10.1016/j.jpowsour.2015.04.117

[35] Pandey G. P., Kumar Y., Hashmi S. A.: Ionic liquid incorporated polymer electrolytes for supercapacitor application. Indian Journal of Chemistry, **49**, 743–751 (2010). http://nopr.niscair.res.in/handle/123456789/9673

[36] Asmara S. N., Kufian M. Z., Majid S. R., Arof A. K.: Preparation and characterization of magnesium ion gel polymer electrolytes for application in electrical double layer capacitors. Electrochimica Acta, **57**, 91–97 (2011). https://doi.org/10.1016/j.electacta.2011.06.045

[37] Bacsik Z., Mink J., Keresztury G.: FTIR spectroscopy of the atmosphere. I. Principles and methods. Applied Spectroscopy Reviews, **39**, 295–363 (2004). https://doi.org/10.1081/ASR-200030192

[38] Hafiza M., Isa M. I. N.: Solid polymer electrolyte production from 2-hydroxyethyl cellulose: Effect of ammonium nitrate composition on its structural properties. Carbohydrate Polymers, **165**, 123–131 (2017). https://doi.org/10.1016/j.carbpol.2017.02.033

[39] Ramlli M., Isa M. I. N.: Structural and ionic transport properties of protonic conducting solid biopolymer electrolytes based on carboxymethyl cellulose doped with ammonium fluoride. The Journal of Physical Chemistry B, **120**, 11567–11573 (2016). https://doi.org/10.1021/acs.jpcb.6b06068

[40] Chai M., Isa M. I. N.: Novel proton conducting solid bio-polymer electrolytes based on carboxymethyl cellulose doped with oleic acid and plasticized with glycerol. Scientific Reports, **6**, 27328/1–27328/7 (2016). https://doi.org/10.1038/srep27328

[41] Arof A. K., Shuhaimi N. E. A., Alias N. A., Kufian M. Z., Majid S. R.: Application of chitosan/iota-carrageenan polymer electrolytes in electrical double layer capacitor (EDLC). Journal of Solid State Electrochemistry, **14**, 2145–2152 (2010). https://doi.org/10.1007/s10008-010-1050-8

[42] Rahaman M. H. A., Khandaker M. U., Khan Z. R., Kufian M. Z., Noor I. S. M., Arof A. K.: Effect of gamma irradiation on poly(vinyledene difluoride)–lithium bis(oxalato)borate electrolyte. Physical Chemistry Chemical Physics, **16**, 11527–11537 (2014). https://doi.org/10.1039/C4CP01233J

[43] Samsudin A. S., Lai H. M., Isa M. I. N.: Biopolymer materials based carboxymethyl cellulose as a proton conducting biopolymer electrolyte for application in rechargeable proton battery. Electrochimica Acta, **129**, 1–13 (2014). https://doi.org/10.1016/j.electacta.2014.02.074

[44] Hamsan M. H., Aziz S. B., Azha M. A. S., Azli A. A., Shukur M. F., Yusof Y. M., Muzakir S. K., Manan N. S. A., Kadir M. F. Z.: Solid-state double layer capacitors and protonic cell fabricated with dextran from *Leuconostoc mesenteroides* based green polymer electrolyte. Materials Chemistry and Physics, **241**, 122290/1–122290/13 (2019). https://doi.org/10.1016/j.matchemphys.2019.122290

[45] Ji Y., Liang N., Xu J., Qu R., Chen D., Zhang H.: Solid polymer electrolyte membranes based on quaternized polysulfone and solvent-free fluid as separators for electrical double-layer capacitors. Electrochimica Acta, **283**, 97–103 (2018). https://doi.org/10.1016/j.electacta.2018.06.156

[46] Shukur M. F., Ithnin R., Kadir M. F. Z.: Electrical characterization of corn starch-LiOAc electrolytes and application in electrochemical double layer capacitor. Electrochimica Acta, **136**, 204–216 (2014). https://doi.org/10.1016/j.electacta.2014.05.075

[47] Shukur M. F., Kadir M. F. Z.: Hydrogen ion conducting starch-chitosan blend based electrolyte for application in electrochemical devices. Electrochimica Acta, **158**, 152–165 (2015). https://doi.org/10.1016/j.electacta.2015.01.167

[48] Lim C-S., Teoh K. H., Liew C-W., Ramesh S.: Capacitive behavior studies on electrical double layer capacitor using poly (vinyl alcohol)–lithium perchlorate based polymer electrolyte incorporated with TiO_2. Materials Chemistry and Physics, **143**, 661–667 (2014). https://doi.org/10.1016/j.matchemphys.2013.09.051

[49] Jacob M. M. E., Arof A. K.: FTIR studies of DMF plasticized polyvinyledene fluoride based polymer electrolytes. Electrochimica Acta, **45**, 1701–1706 (2000). https://doi.org/10.1016/S0013-4686(99)00316-3

[50] Zainuri D. A., Arshad S., Khalib N. C., Razak I. A., Pillai R. R., Sulaiman S. F., Hashim N. S., Ooi K. L., Armaković S., Armaković S. J., Panicker C. Y., Van Alsenoy C.: Synthesis, XRD crystal structure, spectroscopic characterization (FT-IR, ^{1}H and ^{13}C NMR), DFT studies, chemical reactivity and bond dissociation energy studies using molecular dynamics simulations and evaluation of antimicrobial and antioxidant activities of a novel chalcone derivative, (E)-1-(4-bromophenyl)-3-(4-iodophenyl)prop-2-en-1-one. Journal of Molecular Structure, **1128**, 520–533 (2017). https://doi.org/10.1016/j.molstruc.2016.09.022

[51] Gupta S., Varshney P. K.: Effect of plasticizer on the conductivity of carboxymethyl cellulose-based solid polymer electrolyte. Polymer Bulletin, **76**, 6169–6178 (2019). https://doi.org/10.1007/s00289-019-02714-1

[52] Ahmad N. H., Isa M. I. N.: Characterization of unplasticized and propylene carbonate plasticized carboxymethyl cellulose doped ammonium chloride solid biopolymer electrolytes. Carbohydrate Polymers, **137**, 426–432 (2016). https://doi.org/10.1016/j.carbpol.2015.10.092

[53] Chai M. N., Isa M. I. N.: Structural study of plasticized carboxy methylcellulose based solid biopolymer electrolyte. Advanced Materials Research, **1107**, 242–246 (2015). https://doi.org/10.4028/www.scientific.net/AMR.1107.242

[54] Noor N. A. M., Isa M. I. N.: Investigation on transport and thermal studies of solid polymer electrolyte based on carboxymethyl cellulose doped ammonium thiocyanate for potential application in electrochemical devices. International Journal of Hydrogen Energy, **44**, 8298–8306 (2019). https://doi.org/10.1016/j.ijhydene.2019.02.062

[55] Saadiah M. A., Zhang D., Nagao Y., Muzakir S. K., Samsudin A. S.: Reducing crystallinity on thin film based CMC/PVA hybrid polymer for application as a host in polymer electrolytes. Journal of Non-Crystalline Solids, **511**, 201–211 (2019). https://doi.org/10.1016/j.jnoncrysol.2018.11.032

[56] Samsudin A. S., Isa M. I. N.: Structural and ionic transport study on CMC doped NH_4Br: A new types of biopolymer electrolytes. Journal of Applied Sciences, **12**, 174–179 (2012). https://doi.org/10.3923/jas.2012.174.179

[57] Sohaimy M. I. H., Isa M. I. N.: Effect of ammonium carbonate salt concentration on structural and ionic conductivity of cellulose based solid polymer electrolytes. Fibers and Polymers, **16**, 1031–1034 (2015). https://doi.org/10.1007/s12221-015-1031-8

[58] Anbuchudar Azhagan S., Ganesan S.: Effect of ammonium acetate addition on crystal growth, spectral, thermal and optical properties of glycine single crystals. Optik, **123**, 993–995 (2012). https://doi.org/10.1016/j.ijleo.2011.06.063

[59] Lee R. S., Kim D., Pawar S. A., Kim T., Shin J. C., Kang S-W.: van der Waals epitaxy of high-mobility polymorphic structure of Mo_6Te_6 nanoplates/$MoTe_2$ atomic layers with low schottky barrier height. ACS Nano, **13**, 642–648 (2019). https://doi.org/10.1021/acsnano.8b07720

[60] Biswal D. R., Singh R. P.: Characterisation of carboxymethyl cellulose and polyacrylamide graft copolymer. Carbohydrate Polymers, **57**, 379–387 (2004). https://doi.org/10.1016/j.carbpol.2004.04.020

[61] Woo H. J., Majid S. R., Arof A. K.: Conduction and thermal properties of a proton conducting polymer electrolyte based on poly (ε-caprolactone). Solid State Ionics, **199**, 14–20 (2011). https://doi.org/10.1016/j.ssi.2011.07.007

[62] Selvasekarapandian S., Baskaran R., Hema M.: Complex AC impedance, transference number and vibrational spectroscopy studies of proton conducting PVAc–NH_4SCN polymer electrolytes. Physica B: Condensed Matter, **357**, 412–419 (2005). https://doi.org/10.1016/j.physb.2004.12.007

[63] Kamarudin K. H., Isa M. I. N.: Structural and DC ionic conductivity studies of carboxy methylcellulose doped with ammonium nitrate as solid polymer electrolytes. International Journal of Physical Sciences, **8**, 1581–1587 (2013). https://doi.org/10.5897/IJPS2013.3962

[64] Samsudin A. S., Khairul W. M., Isa M. I. N.: Characterization on the potential of carboxy methylcellulose for application as proton conducting biopolymer electrolytes. Journal of Non-Crystalline Solids, **358**, 1104–1112 (2012). https://doi.org/10.1016/j.jnoncrysol.2012.02.004

[65] Selvalakshmi S., Vijaya N., Selvasekarapandian S., Premalatha M.: Biopolymer agar agar doped with NH_4SCN as solid polymer electrolyte for electrochemical cell application. Journal of Applied Polymer Science, **134**, 44702/1–44702/10 (2017). https://doi.org/10.1002/app.44702

[66] Hafiza M. N., Bashirah A. N. A., Bakar N. Y., Isa M. I. N.: Electrical properties of carboxyl methylcellulose/chitosan dual-blend green polymer doped with ammonium bromide. International Journal of Polymer Analysis and Characterization, **19**, 151–158 (2014). https://doi.org/10.1080/1023666X.2014.873562

[67] Park S., Baker J. O., Himmel M. E., Parilla P. A., Johnson D. K.: Cellulose crystallinity index: Measurement techniques and their impact on interpreting cellulase performance. Biotechnology for Biofuels, **3**, 10/1–10/10 (2010). https://doi.org/10.1186/1754-6834-3-10

[68] Sit Y. K., Samsudin A. S., Isa M. I. N.: Ionic conductivity study on hydroxyethyl cellulose (HEC) doped with NH_4Br based biopolymer electrolytes. Research Journal of Recent Sciences, **1**, 16–21 (2012).

[69] Malathi J., Kumaravadivel M., Brahmanandhan G. M., Hema M., Baskaran R., Selvasekarapandian S.: Structural, thermal and electrical properties of PVA–$LiCF_3SO_3$ polymer electrolyte. Journal of Non-Crystalline Solids, **356**, 2277–2281 (2010). https://doi.org/10.1016/j.jnoncrysol.2010.08.011

[70] Chen S., Feng F., Yin Y., Che H., Liao X-Z., Ma Z-F.: A solid polymer electrolyte based on star-like hyperbranched β-cyclodextrin for all-solid-state sodium batteries. Journal of Power Sources, **399**, 363–371 (2018). https://doi.org/10.1016/j.jpowsour.2018.07.096

[71] Teo L., Buraidah M., Nor A., Majid S.: Conductivity and dielectric studies of Li_2SnO_3. Ionics, **18**, 655–665 (2012). https://doi.org/10.1007/s11581-012-0667-2

[72] Govindaraj G., Baskaran N., Shahi K., Monoravi P.: Preparation, conductivity, complex permittivity and electric modulus in AgI-Ag_2O-SeO_3-MoO_3 glasses. Solid State Ionics, **76**, 47–55 (1995). https://doi.org/10.1016/0167-2738(94)00204-6

[73] Prabu M., Selvasekarapandian S., Kulkarni A., Karthikeyan S., Hirankumar G., Sanjeeviraja C.: Structural, dielectric, and conductivity studies of yttrium-doped $LiNiPO_4$ cathode materials. Ionics, **17**, 201–207 (2011). https://doi.org/10.1007/s11581-011-0535-5

[74] Qian X., Gu N., Cheng Z., Yang X., Wang E., Dong S.: Impedance study of $(PEO)_{10}LiClO_4$–Al_2O_3 composite polymer electrolyte with blocking electrodes. Electrochimica Acta, **46**, 1829–1836 (2001). https://doi.org/10.1016/S0013-4686(00)00723-4

[75] Shukur M. F., Ithnin R., Kadir M. F. Z.: Electrical properties of proton conducting solid biopolymer electrolytes based on starch–chitosan blend. Ionics, **20**, 977–999 (2014). https://doi.org/10.1007/s11581-013-1033-8

[76] Stephan A. M., Thirunakaran R., Renganathan N. G., Sundaram V., Pitchumani S., Muniyandi N., Gangadharan R., Ramamoorthy P.: A study on polymer blend electrolyte based on PVC/PMMA with lithium salt. Journal of Power Sources, **81**, 752–758 (1999). https://doi.org/10.1016/S0378-7753(99)00148-2

[77] Shuhaimi N. E. A., Teo L. P., Woo H. J., Majid S. R., Arof A. K.: Electrical double-layer capacitors with plasticized polymer electrolyte based on methyl cellulose. Polymer Bulletin, **69**, 807–826 (2012). https://doi.org/10.1007/s00289-012-0763-5

[78] Bandara T. M. W. J., Mellander B-E.: Evaluation of mobility, diffusion coefficient and density of charge carriers in ionic liquids and novel electrolytes based on a new model for dielectric response. in 'Ionic liquids: Theory, properties, new approaches' (ed.: Kokorin A.) InTech, Rijeka, 383–406 (2011). https://doi.org/10.5772/15183

[79] Yusof Y. M., Illias H. A., Shukur M. F., Kadir M. F. Z.: Characterization of starch-chitosan blend-based electrolyte doped with ammonium iodide for application in proton batteries. Ionics, **23**, 681–697 (2017). https://doi.org/10.1007/s11581-016-1856-1

[80] Lutkenhaus J.: A radical advance for conducting polymers. Science, **359**, 1334–1335 (2018). https://doi.org/10.1126/science.aat1298

[81] Ng L. S., Mohamad A. A.: Protonic battery based on a plasticized chitosan-NH_4NO_3 solid polymer electrolyte. Journal of Power Sources, **163**, 382–385 (2006). https://doi.org/10.1016/j.jpowsour.2006.09.042

[82] Avellaneda C. O., Vieira D. F., Al-Kahlout A., Leite E. R., Pawlicka A., Aegerter M. A.: Solid-state electrochromic devices with Nb_2O_5:Mo thin film and gelatin-based electrolyte. Electrochimica Acta, **53**, 1648–1654 (2007). https://doi.org/10.1016/j.electacta.2007.05.065

[83] Rozali M. L. H., Samsudin A. S., Isa M. I. N.: Ion conducting mechanism of carboxy methylcellulose doped with ionic dopant salicylic acid based solid polymer electrolytes. International Journal of Applied Science and Technology, **2**, 113–121 (2012).

[84] Kamarudin K. H., Rani M. S. A., Isa M. I. N.: Ionic conductivity and conduction mechanism of biodegradable dual polysaccharides blend electrolytes. American-Eurasian Journal of Sustainable Agriculture, **9**, 8–14 (2015).

[85] Hema M., Selvasekerapandian S., Sakunthala A., Arunkumar D., Nithya H.: Structural, vibrational and electrical characterization of PVA–NH_4Br polymer electrolyte system. Physica B: Condensed Matter, **403**, 2740–2747 (2008). https://doi.org/10.1016/j.physb.2008.02.001

[86] Bakar N. Y. A., Muhamaruesa N. H., Aniskari N. A. B., Isa M. I. N. M.: Electrical studies of carboxy methycellulose-chitosan blend biopolymer doped dodecyltrimethyl ammonium bromide solid electrolytes. American Journal of Applied Sciences, **12**, 40–46 (2015). https://doi.org/10.3844/ajassp.2015.40.46

[87] Winie T., Ramesh S., Arof A. K.: Studies on the structure and transport properties of hexanoyl chitosan-based polymer electrolytes. Physica B: Condensed Matter, **404**, 4308–4311 (2009). https://doi.org/10.1016/j.physb.2009.08.004

[88] Raphael E., Avellaneda C. O., Manzolli B., Pawlicka A.: Agar-based films for application as polymer electrolytes. Electrochimica Acta, **55**, 1455–1459 (2010). https://doi.org/10.1016/j.electacta.2009.06.010

[89] Zhu L., Zhu P., Fang Q., Jing M., Shen X., Yang L.: A novel solid PEO/LLTO-nanowires polymer composite electrolyte for solid-state lithium-ion battery. Electrochimica Acta, **292**, 718–726 (2018). https://doi.org/10.1016/j.electacta.2018.10.005

[90] Singh R., Polu A. R., Bhattacharya B., Rhee H-W., Varlikli C., Singh P. K.: Perspectives for solid biopolymer electrolytes in dye sensitized solar cell and battery application. Renewable and Sustainable Energy Reviews, **65**, 1098–1117 (2016). https://doi.org/10.1016/j.rser.2016.06.026

[91] Rasali N., Nagao Y., Samsudin A. S.: Enhancement on amorphous phase in solid biopolymer electrolyte based alginate doped NH_4NO_3. Ionics, **25**, 641–654 (2018). https://doi.org/10.1007/s11581-018-2667-3

[92] Monisha S., Mathavan T., Selvasekarapandian S., Benial A. M. F., Aristatil G., Mani N., Premalatha M., Vinoth pandi D.: Investigation of bio polymer electrolyte based on cellulose acetate-ammonium nitrate for potential use in electrochemical devices. Carbohydrate Polymers, **157**, 38–47 (2017). https://doi.org/10.1016/j.carbpol.2016.09.026

[93] Kadir M. F. Z., Salleh N. S., Hamsan M. H., Aspanut Z., Majid N. A., Shukur M. F.: Biopolymeric electrolyte based on glycerolized methyl cellulose with NH_4Br as proton source and potential application in EDLC. Ionics, **24**, 1651–1662 (2018). https://doi.org/10.1007/s11581-017-2330-4

[94] Li J., Lian K.: Investigation of hydroxide ion-conduction in solid polymer electrolytes via electrochemical impedance spectroscopy. Electrochimica Acta, **288**, 1–11 (2018). https://doi.org/10.1016/j.electacta.2018.08.059

[95] Genovese M., Wu H., Virya A., Li J., Shen P., Lian K.: Ultrathin all-solid-state supercapacitor devices based on chitosan activated carbon electrodes and polymer electrolytes. Electrochimica Acta, **273**, 392–401 (2018). https://doi.org/10.1016/j.electacta.2018.04.061

[96] Kumar Y., Pandey G., Hashmi S.: Gel polymer electrolyte based electrical double layer capacitors: Comparative study with multiwalled carbon nanotubes and activated carbon electrodes. The Journal of Physical Chemistry C, **116**, 26118/1–26118/10 (2012). https://doi.org/10.1021/jp305128z

[97] Singh R., Bhattacharya B., Gupta M., Rahul, Khan Z. H., Tomar S. K., Singh V., Singh P. K.: Electrical and structural properties of ionic liquid doped polymer gel electrolyte for dual energy storage devices. International Journal of Hydrogen Energy, **42**, 14602–14607 (2017). https://doi.org/10.1016/j.ijhydene.2017.04.126

[98] Kadir M. F. Z., Aspanut Z., Majid S. R., Arof A. K.: FTIR studies of plasticized poly(vinyl alcohol)–chitosan blend doped with NH_4NO_3 polymer electrolyte membrane. Spectrochimica Acta Part A: Molecular and Biomolecular Spectroscopy, **78**, 1068–1074 (2011). https://doi.org/10.1016/j.saa.2010.12.051

[99] Hashmi S., Latham R. J., Linford R. G., Schlindwein W. S.: Studies on all solid state electric double layer capacitors using proton and lithium ion conducting polymer electrolytes. Journal of the Chemical Society, Faraday Transactions, **93**, 4177–4182 (1997). https://doi.org/10.1039/A704661H

[100] Arof A. K., Shuhaimi N. E. A., Amirudin S., Kufian M. Z., Woo H. J., Careem M. A.: Polyacrylonitrile–lithium bis(oxalato) borate polymer electrolyte for electrical double layer capacitors. Polymers for Advanced Technologies, **25**, 265–272 (2014). https://doi.org/10.1002/pat.3231